International Journal of Neural Systems, Vol. 30, No. 10 (2020) 2050053 (16 pages)

DOI: 10.1142/S0129065720500537

Improved Activity Recognition Combining Inertial Motion Sensors and Electroencephalogram Signals

Manuel Graña*, Marina Aguilar-Moreno*, Javier De Lope Asiain†,‡,
Ibai Baglietto Araquistain*,and Xavier Garmendia*
*Computational Intelligence Group
University of the Basque Country (UPV/EHU),
San Sebastian, Spain
†Department of Artificial Intelligence
Universidad Politécnica de Madrid (UPM),
Madrid, Spain
‡javier.delope@upm.es

Accepted 20 June 2020
Published Online 11 September 2020

Human activity recognition and neural activity analysis are the basis for human computational neureoethology research dealing with the simultaneous analysis of behavioral ethogram descriptions and neural activity measurements. Wireless electroencephalography (EEG) and wireless inertial measurement units (IMU) allow the realization of experimental data recording with improved ecological validity where the subjects can be carrying out natural activities while data recording is minimally invasive. Specifically, we aim to show that EEG and IMU data fusion allows improved human activity recognition in a natural setting. We have defined an experimental protocol composed of natural sitting, standing and walking activities, and we have recruited subjects in two sites: in-house ($N = 4$) and out-house ($N = 12$) populations with different demographics. Experimental protocol data capture was carried out with validated commercial systems. Classifier model training and validation were carried out with scikit-learn open source machine learning python package. EEG features consist of the amplitude of the standard EEG frequency bands. Inertial features were the instantaneous position of the body tracked points after a moving average smoothing to remove noise. We carry out three validation processes: a 10-fold cross-validation process per experimental protocol repetition, (b) the inference of the ethograms, and (c) the transfer learning from each experimental protocol repetition to the remaining repetitions. The in-house accuracy results were lower and much more variable than the out-house sessions results. In general, random forest was the best performing classifier model. Best cross-validation results, ethogram accuracy, and transfer learning were achieved from the fusion of EEG and IMUs data. Transfer learning behaved poorly compared to classification on the same protocol repetition, but it has accuracy still greater than 0.75 on average for the out-house data sessions. Transfer leaning accuracy among repetitions of the same subject was above 0.88 on average. Ethogram prediction accuracy was above 0.96 on average. Therefore, we conclude that wireless EEG and IMUs allow for the definition of natural experimental designs with high ecological validity toward human computational neuroethology research. The fusion of both EEG and IMUs signals improves activity and ethogram recognition.

Keywords: Neuroethology; activity recognition; EEG; inertial measurement.

‡Corresponding author.

1. Introduction

There is a plethora of approaches for human activity measurement and recognition using diverse sensors. Computer vision techniques based on conventional video[1] and depth cameras[2,3] have been extensively applied. Machine learning techniques[4] over data from wearable motion tracking devices based on inertial measurement units (IMUs)[5–9] are another major research line, including their use for medical purposes.[10] Diverse feature extraction methods have been proposed, such as the fractal dimension[11] for the characterization of walking path tortuosity of aging person, space-time representations of actions,[12] or the application of conditional random fields[13] for human motion recognition. Information fusion for human activity recognition[14–16] has targeted the combination of same kind sensors. We have not found works using the fusion of neural and body motion sensors along the lines of the work that we are reporting in this paper.

Human activity recognition is arguably the human equivalent of computational ethology,[17] defined as the extensive use of computers and digitalized sensors for animal behavior observation, quantification, and analysis. A central tool in computational ethology is the ethogram, which is a quantitative representation of the measured behavior that can be used for the supervised or unsupervised classification of behaviors, quantitative comparisons, and detection of anomalies. Ethograms take the form of time plots of the observed activity identifiers inferred from sensor data. Computational ethology has made extensive use of image processing and computer vision techniques[18] for remote identification and tracking[19,20] of individuals in isolated[21] or social contexts.[22,23] The field is mature to the point of commercial software/hardware bundles for specific applications.[24,25] Besides, computational ethology uses a wide variety of sensors, such as structured light,[20] X-ray imaging for animals embedded in the soil, thermal imaging for video shooting in darkness,[26] sonar signals for underwater monitoring, sensitive pressure sensors for micro-motion detection,[27] catwalk systems for animal gait analysis,[28] as well as innovative machine learning for automated construction of ethograms, such as the convolutional neural networks (CNN),[29–31] spatiotemporal bags of words,[26] and data compression.[32]

Electroencephalography (EEG) is an electrophysiological measurement that allows to infer measurements of the activity in the brain[33] used in many neuroscience and cognitive psychological studies.[33–38] Often, cognitive experiments impose very stringent conditions (sitting very quietly while carrying a repetitive task) on the subject that diminish the ecological validity of the study. In psychology, the ecological validity[39] of a study relates to how the materials and setting of the study mirror the real-world effects are targeted by the study. Wireless EEG devices[40,41] with high reliability[42] allow new experimental designs where the subject is allowed some freedom of movement. Some animal models are successful demonstrators of the wireless EEG technology.[43,44] Also, it has been proposed for clinical trials[45] with applications in epilepsy diagnosis and follow up. Monitoring neural activity while wandering in an art museum has been reported.[46] Moreover, robust and sensitive dry electrodes[41,47] are easier to deploy on inexperienced subjects. We benefit from these resources in order to improve the ecological validity of our activity recognition experiments based on EEG and IMUs recordings.

Neuroethology deals with the study of animal behavior and the latent nervous system mechanisms controlling it, emphasizing the evolutive and comparative aspects in natural settings.[48] On some lower animals, empirical computational neuroethological experiments are based on the ability to manipulate their neural pathways and the detailed observation of the ensuing behavior.[49] On higher animals, objective measurement of behavior carried by computational ethology means can be correlated to brain circuits via postmortem histology, or via *in vivo* measurement of neural activity by EEG using electrode implants or functional Magnetic Resonance Imaging (fMRI). Some recent higher animal study examples are the compression of the spinal cord,[50] hypoxia-ischemia in newborns,[51] and fear.[52] There are also examples of human neuroethology using fMRI for neural activity reading synchronized with the behavioral responses, such as a human fear model,[52] and the highly abstract simulation of foraging behaviors in Ref. 53. However, ecological validity of fMRI studies is rather poor. Some works use physiological sensors to infer internal states of the human subject, such as stress level,[54] however EEG provides much more direct evidence.[55,56] Wireless EEG

devices allow much more natural experiences such as joint recording of body motion and the EEG of piano player while performing a simple tune.[57] We postulate that the experimental works reported in this paper fall near the domain of human computational neuroethology.

Our main working hypothesis is that fusing the information body motion tracking devices and EEG would allow improved recognition of the instantaneous subject state in an experimental protocol, and of the overall ethogram. We translate this hypothesis into a classification problem: the fusion of neural activity and body motion data will improve activity recognition by trained classifiers. In this paper, we define an experimental protocol carried out by recruited subjects in two experimental sites. We use wireless EEG recording and IMUs body points trajectory tracking at each data capture session. We extract behavioral and neural activity features for instantaneous classification and inference of the subject ethogram corresponding to the protocol repetition data capture. In this regard,[58] the provided preliminary evidence shows that the combined neural and behavioral information improve activity recognition results on a simple protocol. This paper improves over these results on a larger population carrying out a more complex activity experimental protocol. We use off-the-shelf recording equipment and open source machine learning implementations in order to capture the data and process it. Results show improved ethogram prediction from the fusion of the inertial and neural activity data.

2. Materials and Methods

2.1. *Experimental populations*

We have carried out two batches of experimental data capture with the software published in [59]. The first experimental capture batch, that we call in-house experiment, was carried out in a seminar room of the Computer Science School, mostly devoid of running computational equipment. The five enrolled subjects were senior researchers. The second, the out-house experiment, was realized with the collaboration of a Local Technological School (Instituto de Maquina Herramienta IMH) involved in a locally funded research project referred below, were we were able to engage 12 subjects to carry out data collection sessions. All subjects signed an informed consent. The data capture process was supervised and approved by the IMH teaching staff. After data collection, some of the protocol repetitions were rejected. Causes of rejection were excessive drift of the IMUs measurements (above 5% in all sensors), and low quality signal for more than 10% of the protocol duration of the EEG sensor readings. At the end of the day, we got 25 protocol repetitions for analysis and report.

2.2. *Data sources*

2.2.1. *Body motion capture*

For the quantitative observation of the subject's behavior, we use the rokoko motion capture suit.[a] Figure 1 shows the schema of the central hub collecting the information from the nine degrees of freedom IMUs, and forwarding it via wifi connection to the host computer, and the placement of the IMUs on the body. The IMUs are embedded in the textile suit, which can be tightly adjusted to minimize noisy readings from involuntary random motions because of that, the suit does not need any anatomical calibration. The suit calibration for a data recording

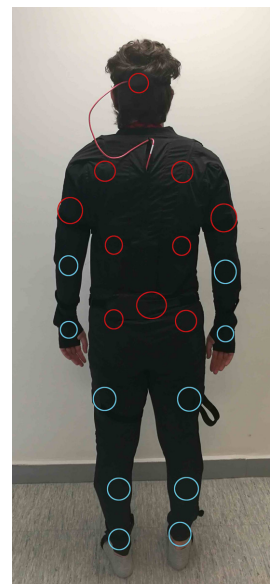

Fig. 1. (Color online) Rokoko elements. The placement of the sensors in the suit. Blue circles correspond to sensors placed at the front of the suit. Red circles correspond to sensors placed at the back of the suit.

[a]https://www.rokoko.com/.

session requires the subject to be still for a few seconds. The sampling frequency is 100 Hz. The rokoko suit suffers from drifting effects in laboratory conditions where there are many electromagnetic sources affecting the IMU sensors. For this reason, the data capture experiments have been carried out in rooms devoid of working active electrical devices. The suit contains 19 IMUs whose readings allow to compute the 3D coordinates and orientation of 25 points distribute over the body, head, and arms.

2.2.2. *Neural activity capture*

The second data source is the neural activity measurement by a wireless EEG sensor, namely, the 8 electrode enobio (Neuroelectrics,[b] Cambridge, MA). The wireless connection allows natural activities, so subjects can move around, sit down and make other natural movements. Figure 2(a) shows the actual cap with the wearable box containing the signal concentrator, and the wireless emitter for communication with host computer. Figure 2(b) shows the actual location of the electrodes in the standard map of EEG channels. We placed them over the occipital, temporal, and frontal lobes in order to try to capture the differences among the diverse activities described below. Temporal (T7, T8) and occipital (O1, O2) electrodes would allow to discriminate auditory and visual tasks. The prefrontal electrode (FPz) and the frontal electrodes (F3, Fz, F4) would allow to discriminate passive tasks from tasks involving planning and decision making, as well as some kind of motor planning and coordination. We have used the dry electrodes shown in Fig. 2(c) that do not need any kind of gel or saline solution. Dry electrodes are very convenient for subjects not accustomed to EEG sessions, increasing the ecological validity of the study. The enobio control and data capture program allow visualization of the signal in real time. We have used its event scheduling for the accurate scheduling of the activities carried out by the subjects. The quality of the signal is monitored online and some well-known artifacts, e.g. blinking, are removed automatically by the signal capture software. The sampling rate is 500 Hz. We apply a bandpass filter at 0.1–50 Hz (FIR, Hamming, 60 db) ensuring that the most important neural frequency bands from alpha to gamma are

[b]www.neuroelectrics.com.

(a)

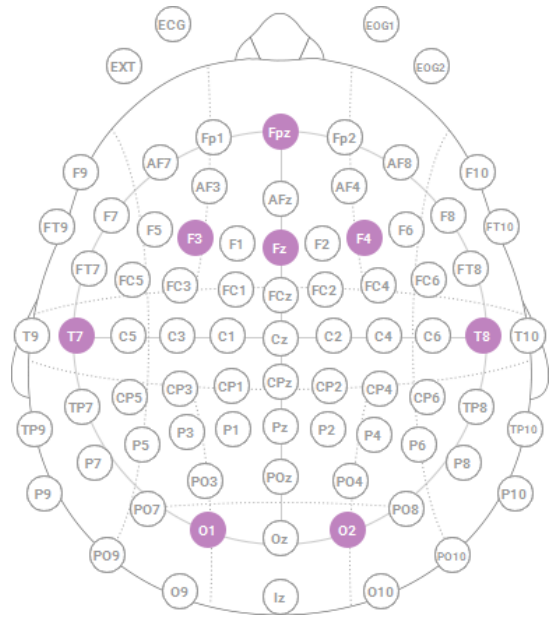

(b)

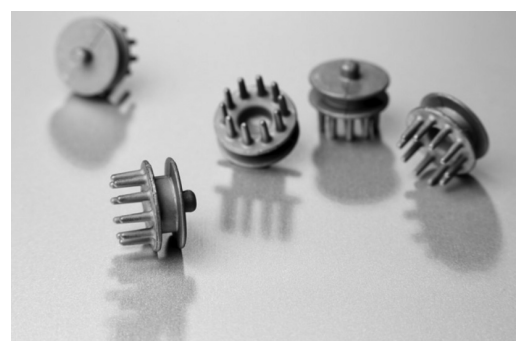

(c)

Fig. 2. The enobio wireless EEG sensor. (a) The cap with the electrode signal concentrator and the wireless emitter, (b) the location of the channels recorded for our experiment, (c) the dry electrodes used in the experiment.

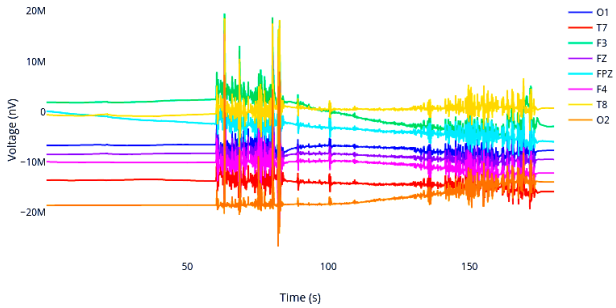

Fig. 3. Plots of the raw signal of the enobio EEG channels for one repetition of the experimental protocol by one of the participants.

preserved. Finally, the signal is subsampled at 100 Hz fulfilling the conditions of the Nyquist–Shannon sampling theorem. Figure 3 shows the multiple plots of the EEG channel signals on their relative head location. The signal values have been normalized to the overall signal mean over all channels.

2.3. *Experimental protocol*

The experimental protocol is carried out twice by each subject. Its timing is controlled by enobio base software. Figure 4 illustrates the spatial configuration of the protocol. Circles with numbers correspond to the protocol steps described below, their position corresponds to the relative motions of the subject.

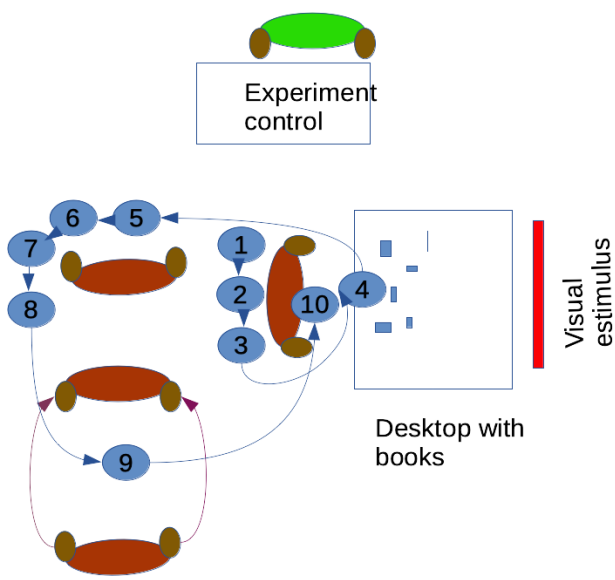

Fig. 4. Experimental protocol activity flow. Circles with numbers corresponds to the steps of the protocol steps described in the text.

Before each protocol repetition, the subject is asked to remain standing still for several seconds in order to calibrate the rokoko suit. The protocol steps and durations are as follows:

(1) Subject seated relaxed in front of a table — 20 s.
(2) Visual task: An abstract colorful painting is shown in front of he subject's face at eye level — 20 s.
(3) Auditive task (eyes closed are recommended): Listening to Mozart's Piano Concerto N. 21 in C Major — 20 s.
(4) Moving around and organizing the objects (books) on the top of the table — 20 s.
(5) Standing up and waiting — 10 s.
(6) Subject makes waving and salute motions with the right hand — 20 s.
(7) Clapping — 20 s.
(8) Pushing ahead with arms and hands — 20 s.
(9) Walking in straight line forward and backward — 20 s.
(10) Sitting down and standing all movement — 10 s.

The experimental protocol involves all the selected brain regions, and the IMU readings along the body. It includes some resting states, namely steps 1, 5, and 10. However, they have different body kinematics and dynamics. Step 1 is the baseline resting state without motion while seated; step 5 corresponds to the motion reaching a standing position which involves some equilibrium control; step 10 involves reaching the chair, sitting down, and relaxing to achieve the resting state. Steps 2 and 3 involve sensory processing of different kinds which would activate different brain areas (temporal and occipital) that should be easily discriminated. Step 4 involves planning and decision making while moving the arms, so the frontal lobe will be more active. Steps 6–8 involve different arm motions while standing, deciding how to perform the motions as well as the motor control will activate the frontal lobe in a different way. Finally, step 9 involves full body motion and planning of this motion.

2.4. *Feature extraction*

Both IMU and EEG sensor data are sampled at 100 Hz. Data capture synchronization is achieved by

simultaneous recording start pressing a key. Hence, we assume that the time stamps of samples from both sensors are in the same time frame. Each time instant is labeled with the number of the activity the subject is engaged in, i.e. $Y_i = \{y_t\}_{t=0}^{T}$, where $i \in \{1, \ldots, N\}$ is the trial number, T is the duration of the protocol trial in seconds, and $y_t \in \{1, \ldots, 10\}$. The nominal duration of the protocol repetitions is $T = 180$ s. The actual duration of the protocol steps has small variations due to subject variability between repetitions, introducing label errors at the time limits of the protocol steps. The EEG signals are centered by subtracting the mean of all EEG signals. We do not decompose the EEG signal into epochs. We apply bandpass filters (FIR, Hamming, 60 db) to obtain the amplitude at the Delta (0.1–4 Hz), Theta (4–7 Hz), Alpha (8–15 Hz), Beta (16–31 Hz), Gamma (30–50 Hz) bands. Therefore, the EEG trial data is denoted by $X_i^E = \{\mathbf{x}_{i,t}^E\}_{t=0}^{T}$, where $\mathbf{x}_{i,t}^E \in \mathbb{R}^{40}$.

The inertial sensors provide the 3D position estimation of 25 points over the body. To smooth the inertial recordings, we compute a moving average of the body point trajectories over a window spanning 0.1 s. The extracted features consist in the first-order time differences of the smoothed signal, denoted $X_i^I = \{\mathbf{x}_{i,t}^I\}_{t=0}^{T}$, where $\mathbf{x}_{i,t}^I \in \mathbb{R}^{75}$.

We consider three kinds of feature datasets for training and validation: (a) only the EEG data X_i^E, (b) only the inertial data X_i^I, and (c) the fusion of both denoted by $X_i^{E+I} = \{[\mathbf{x}_{i,t}^E, \mathbf{x}_{i,t}^I]\}_{t=0}^{T}$, i.e. when the feature vectors are the composition of the data vectors of both modalities. Finally, the signals are downsampled at 10 Hz to build up the feature datasets for training and validation of the classifiers.

2.5. *Classification models*

Our main working hypothesis is that the combined use of body motion tracking and neural activity would allow improved recognition of the subject's actual activity. We translate this hypothesis into a classification problem: Does the fusion of neural activity and body motion data improve activity recognition?. Therefore, we have used a machine learning approach testing several classifiers available from the scikit-learn python package.[c] We used the following well-known classifier building models:

- Gaussian Naive Bayes (NB)[60] assumes the statistical independence of the features, so that the overall classifier is built as the aggregation of the scalar independent classifiers defined for each feature. Each classifier is modeled by a mixture of Gaussians.
- K-Nearest Neighbors (Knn) Classifier[60] ($K = 5$). The class is assigned as the majority class of the K training samples which are closest to the input feature vector according to the Euclidean distance.
- Decision Tree (DT) is the classical nonparametric supervised training technique[61] which proceeds by a sequence of decisions, each one of them defined as the optimal split of the data according to some information theoretic criterion, e.g. the Gini index.
- Random forest (RF)[62] (#trees = 1000) is an ensemble of DT classifiers where each split is computed on randomized selections of the features.
- Gradient Boosting (GB)[63] (#boosting stages = 1000) is an additive ensemble built incrementally following a greedy strategy to minimize the loss, at each stage a regression tree is fit to the negative gradient of the loss function.

The rationale for the choice of the classifier models is as follows: we want to show that the fusion of neural and motion information leads to improved recognition of the activity the subject is engaged in. We are interested in assessing whether this improvement happens for various classifiers. On the one hand, we have selected the RF, which is recognized as a top performing classifier building approach,[64,65] and GB which has also achieved top performance in neurorobotics tasks.[66] On the other hand, we selected Knn and NB as simple classifiers that are often reported as the baseline classifiers.[67] We have applied the default setting of parameters for each classifier because exhaustive classifier behavior analysis is not the aim of the work.

2.6. *Validation processes*

We have carried out the following validation processes:

- First, we consider each trial by a subject as an independent dataset. We consider for comparison the three kinds of feature vectors defined above, i.e. the feature datasets are $\{X_i^E, Y_i\}$,

[c]https://scikit-learn.org/.

$\{X_i^I, Y_i\}$, and $\{X_i^{E+I}, Y_i\}$, where $i \in \{1, \ldots, N\}$ is the protocol repetition number. For each feature dataset $\{X_i^*, Y_i\}$, where $*$ can be I, E, or $E + I$, we carry out a 10-fold cross-validation experiment as follows: We partition the feature dataset into 10 folds $\{X_{i,k}^*, Y_{i,k}\}_{k=1}^{10}$ obtained by stratified sampling without replacement, therefore folds do not preserve the time stamp order of the samples. Then we alternatively use each fold $\{X_{i,w}^*, Y_{i,w}\}; w = 1, \ldots, 10$ as the test data to validate a classifier $\phi_{i,w}^*$ built using the remaining folds $\{X_{i,k}^*, Y_{i,k}\}_{k \neq w}$ as the training data. For each protocol repetition, we report the average performance measure achieved by the classifiers $\{\phi_{i,w}^*\}_{w=1}^{10}$. The reported performance measure is the accuracy computed as the ratio of the correct predictions to the dataset size, i.e. $A_{i,w}^* = |\{Y_{i,w}\}|^{-1} \sum_{t \in T_w} \delta(y_t - \phi_{i,w}^*(x_{i,t}^*))$, where T_w denotes the time stamps of samples in the kth fold, $\delta()$ is the delta function defined as $\delta(0) = 1; \delta(x \neq 0) = 0$, and $|Y|$ denotes the size of set Y.

- Second, we treat the data sequentially, predicting the ethogram of each protocol trial from each of the feature vectors considered. The classifier applied to the computation of the ethogram is the best one found in the cross-validation experiment for each trial, i.e. we use $\phi_{i,w'}^*; w' = \arg\max_w A_{i,w}^*$. We do not use temporal dependencies in the classification, neither we apply any post-processing on the classification responses. In other words, we compute $\hat{Y_i^*} = \{\hat{y}_t = \phi_{i,w'}^*(x_{i,t}^*)\}_{t=0}^T$. Ethogram accuracy is defined similarly as above.
- Third, we consider the problem of direct transfer learning using all the features, i.e. the application of the best classifier $\phi_{i,w'}^{E+I}$ trained over $\{X_i^{E+I}, Y_i\}$ to the remaining protocol repetitions $\{X_j^{E+I}, Y_j\}; j \neq i$. We want to assess to what extent it is possible to generalize the action recognition classifier learnt from one protocol repetitions. We apply a post-processing correction consisting in selecting the majority activity label over a time window of 0.1 s of size centered at each instant. Denoting $\hat{Y}_j^i$ the ethogram of the jth protocol repetition obtained by applying the classifier trained on the ith protocol repetition, the corresponding transfer learning accuracy is defined as $A_j^i = |\{Y\}|^{-1} \sum_t \delta(y_t - \phi_{i,w'}^{E+I}(x_{j,t}^{E+I}))$.

3. Results and Discussion

3.1. *In-house trials experimental results*

Figure 5 presents the summary accuracy results of the cross-validation processes computed independently over each protocol repetition data. Figure 5(a) plots the mean accuracy achieved by the selected classifiers over all repetitions for the different definitions of feature vectors: IMUs, EEG, and the fusion of both. Figure 5(b) plots the variance of the accuracy. The use of the sensor data fusion features results in a great reduction of variance in accuracy performance. First conclusion is that the fusion of IMUs and EEG features achieves the best results. (F test, $p < 0.01$, one-sided t-tests $A^{E+I} > A^I$ $p < 0.01$, and $A^{E+I} > A^E$ $p < 0.01$). Figure 5(d) shows the differences in average accuracies for the feature selection $A^{E+I} - A^I$, and $A^{E+I} - A^E$, which confirms this conclusion. The classifiers that achieve best average accuracy are the RF and the GB (F test, $p < 0.01$, one-sided t-tests comparing classifiers $p < 0.01$ when comparing RF or GB against Knn, DT, or NB, two-sided t-test comparing RF and GB $p > 0.1$). Figure 5(c) plots the average accuracies over the classifiers per protocol repetition. It is possible to assess the great variability of the results over the protocol repetitions. Missing plots correspond to discarded protocol repetitions.

Figure 6 shows the ethograms inferred from each protocol repetition data. Real ethograms have a staircase shape because the subject advances linearly on the protocol steps. Confusions can be identified as the red dots that appear outside the staircase. Figure 6(a) shows the ethograms inferred from the EEG data. It can be appreciated that confusions are greater in the last part of the protocol, where the subject is moving. These confusions are greatly subject dependent, apparently because of diverse motion patterns among individuals. Figure 6(b) corresponds to the inertial measurements, where we find that most of the confusion happens during the first steps of the protocol, which are mostly static activities. The ethograms inferred from the fusion of the inertial and EEG data are shown in Fig. 6(c). The improvement achieved in activity prediction is clear. Sensor data fusion allows to correct great percentage of confusions. These ethograms are shown without

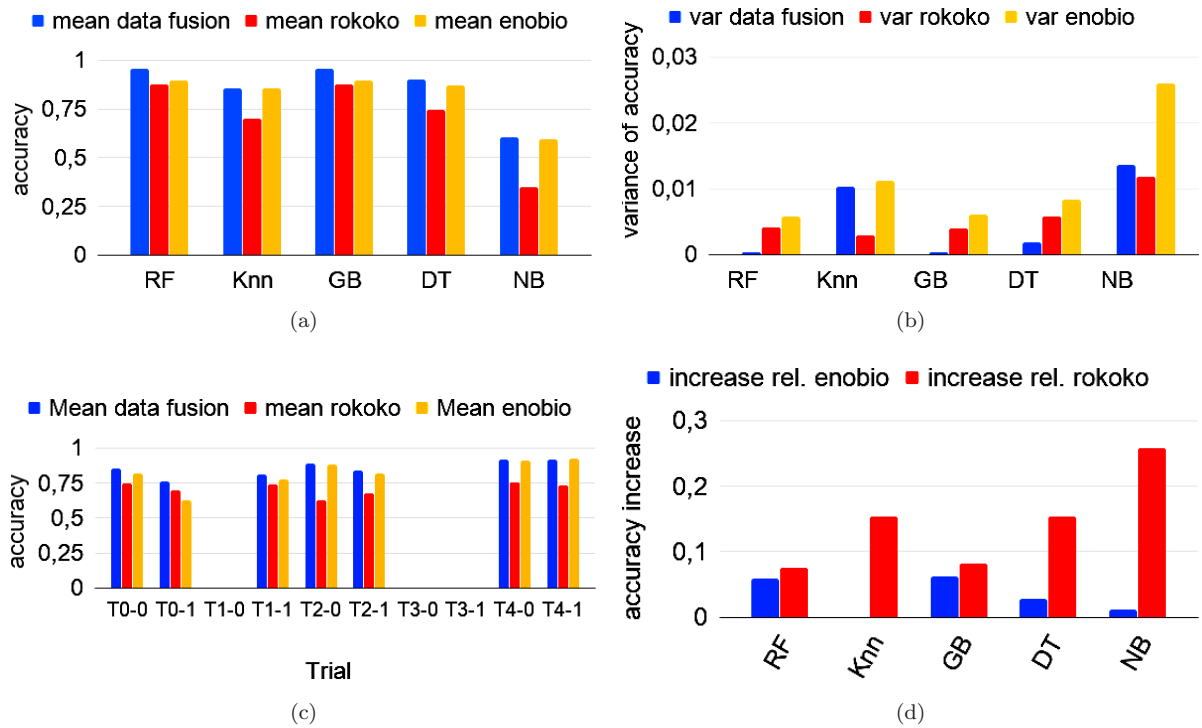

Fig. 5. Summary results of the in-house trials cross-validation experiments. (a) Average accuracy achieved by the classifiers over either the EEG (enobio), inertial (rokoko), or the fusion of both modalities (enobio+rokoko), (b) variance of the accuracy results per classifier, (c) average accuracy achieved per repetition of the experimental protocol (repetitions are denoted Tx-y, where x subject id, y repetition number). (d) accuracy improvement achieved by data fusion relative to either the EEG or the inertial data. (RF = random forest, Knn = K nearest neighbors, GB = gradient boosting, DT = decision tree, NB = Naive Bayes).

temporal post-processing. The accuracy of ethogram prediction after temporal post-processing correction is presented in the diagonal of Table 1, which reports transfer learning results for the in-house experiment. Note that the table is not symmetric because classifiers from symmetric entries may behave differently on their respective symmetric dataset. The diagonal corresponds to the ethogram inference on the same dataset, its mean accuracy is 0.90, and its standard deviation is 0.07, a rather large value that reflects the accuracy results of diagonal correspond to the transfer learning, which is significantly lower (mean = 0.74) than the nontransfer accuracy (two sample t-test, $p < 0.0001$).

3.2. *Out-house experimental results*

The accuracy performance results of the 10-fold cross-validation over the data from the out-house experiment realized at the IMH are summarized in Fig. 7. Figure 7(a) plots the mean accuracy achieved by the selected classifiers over all repetitions for the different definitions of feature vectors: IMUs, EEG, and the fusion of both. Figure 7(b) plots the variance of the accuracy estimation. The use of the IMUs and EEG sensor fusion features results in a great reduction of variance in accuracy performance for all classifiers except NB. Sensor fusion features achieve the highest accuracy results. (F test, $p < 0.01$, one-sided t-tests $A^{E+I} > A^I$, $p < 0.01$, and $A^{E+I} > A^E$, $p < 0.01$). Figure 7(d) shows the differences in average accuracies $A^{E+I} - A^I$, and $A^{E+I} - A^E$, which confirms the previous conclusion. The classifiers that achieve best average accuracy are the RF and the GB (F test, $p < 0.01$, one-sided t-tests comparing classifiers $p < 0.01$ when comparing RF or GB against Knn, DT, or NB, two-sided t-test comparing RF and GB result $p > 0.1$). Figure 7(c) plots the average accuracies over the classifiers per protocol repetition. It is possible to assess the variability of the results over the protocol repetitions, though it is less that in the in-house case. The inertial measurement results in greater variability than EEG and sensor fusion

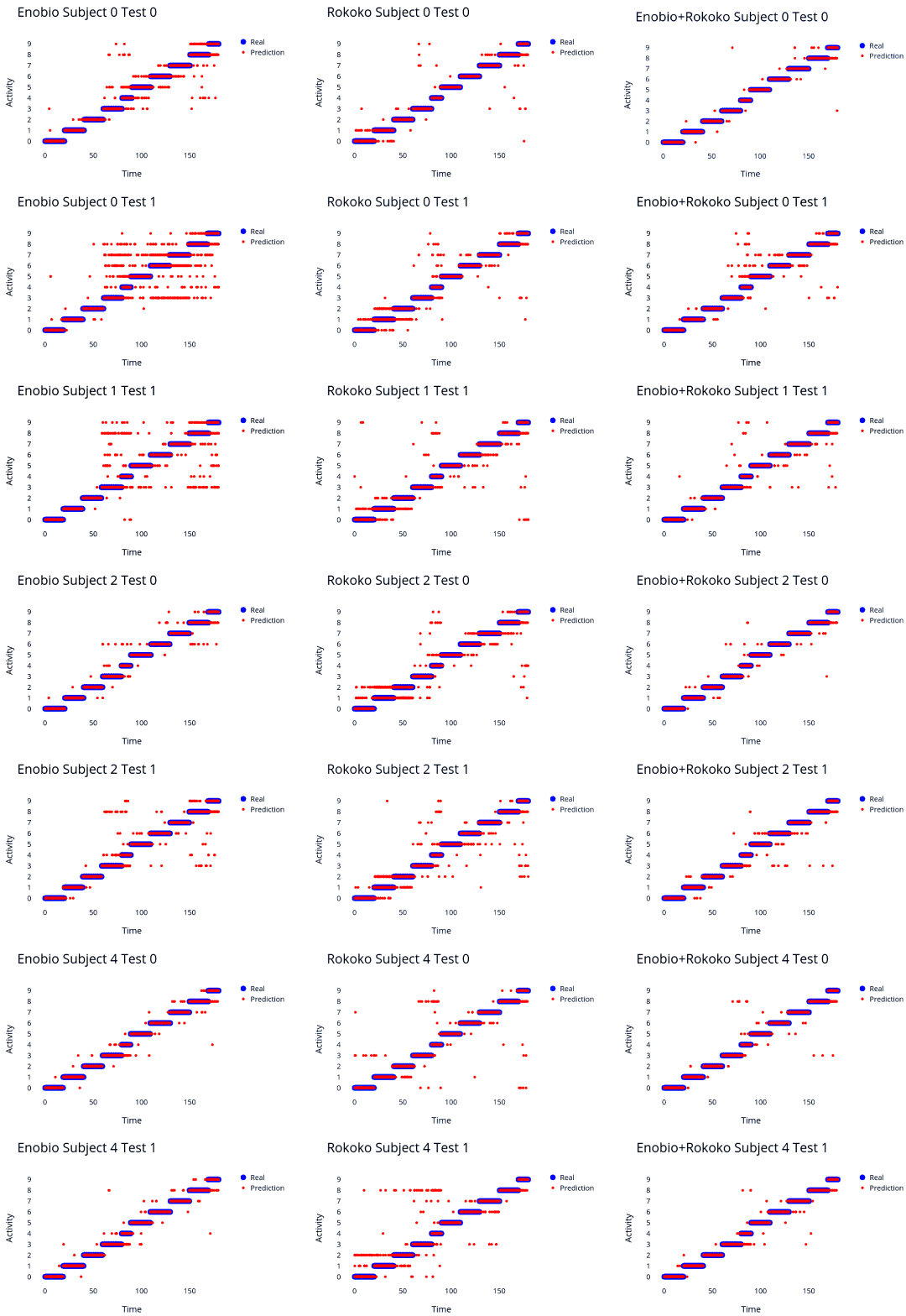

Fig. 6. Ethogram prediction from the in-house trials based on (a) EEG (enobio) data, (b) inertial (rokoko) data, (c) fusion of EEG and inertial data. No post-processing correction was applied.

Table 1. Transfer learning results for the in-house protocol repetitions. Each row corresponds to the accuracy achieved applying the best classifier trained on the data of the trial to the remaining trials. Trials are denoted Tx-y, x = subject id, y = trial number. Post-processing correction was applied.

	T0-0	T0-1	T1-1	T2-0	T2-1	T4-0	T4-1
T0-0	0.97	0.84	0.73	0.71	0.72	0.69	0.69
T0-1	0.82	0.89	0.75	0.70	0.72	0.70	0.70
T1-1	0.72	0.73	0.90	0.77	0.75	0.71	0.69
T2-0	0.7	0.71	0.79	0.82	0.80	0.77	0.78
T2-1	0.69	0.68	0.75	0.83	0.88	0.79	0.80
T4-0	0.7	0.71	0.72	0.79	0.80	0.95	0.91
T4-1	0.73	0.73	0.70	0.78	0.79	0.90	0.93

features. We note that DT, NB, and Knn classifiers did not show any improvement of the accuracy between the EEG data and the sensor fusion data (two-sided t-test $p > 0.1$). All classifiers show significant accuracy improvement of the sensor fusion over the inertial measurements only (F test, $p < 0.01$, pairwise comparisons with one-sided t-test $p < 0.01$).

Exhaustive plotting of the ethograms of the IMH protocol repetitions, such as in Fig. 6, is unwieldy, therefore we provide in Fig. 8 a summary visualization of the results. Figure 8(a) plots the number of correct hits (correct predictions) per protocol activity. The lower number of hits achieved in protocol activities #5 and #10 might be due to their shorter time duration. The number of hits on sitting activities (#1–#4) is lower for the inertial data than for the EEG and sensor fusion features. However, inertial data slightly improve over EEG data on the moving around activities (#6–#9). On all activities, the sensor fusion data provide the upper number of hits. Figures 8(b)–8(d) visualize the average confusion matrices obtained from the inertial, EEG, and sensor fusion features, respectively. Sensor fusion features produce lower confusion matrices (pairwise one-sided t-tests among confusion matrices $p < 0.01$).

Transfer learning results for the out-house protocol repetitions are reported in Table 2. The table is not symmetric. The diagonal values correspond to

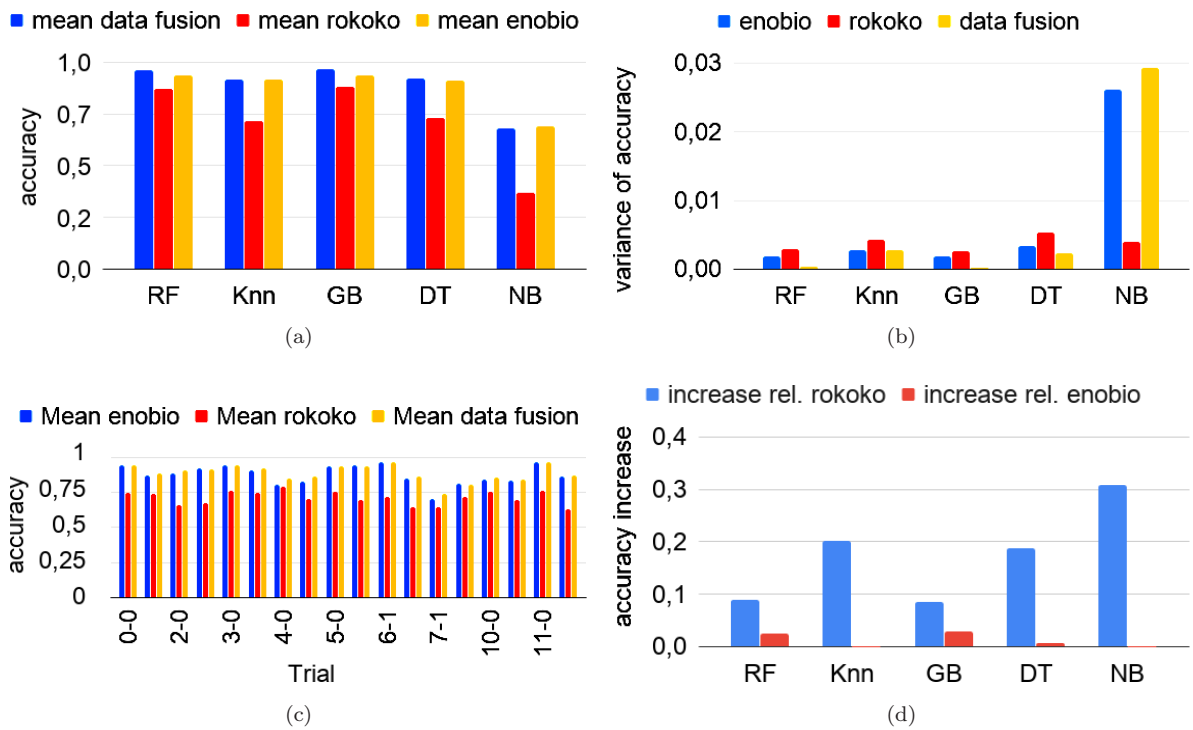

Fig. 7. Out-house data capture experiment summary classification results. (a) Average accuracy achieved by the classifiers on the EEG (enobio), inertial (rokoko), and sensor fusion data, (b) variance of the accuracy results per classifier, (c) average accuracy achieved per repetition of the experimental protocol (denoted Tx-y, x subject id, y repetition number), (d) improvement achieved by data fusion relative to either the EEG or the inertial data. (RF = random forest, Knn = K-nearest neighbors, GB = gradient boosting, DT = decision tree, NB = Naive Bayes).

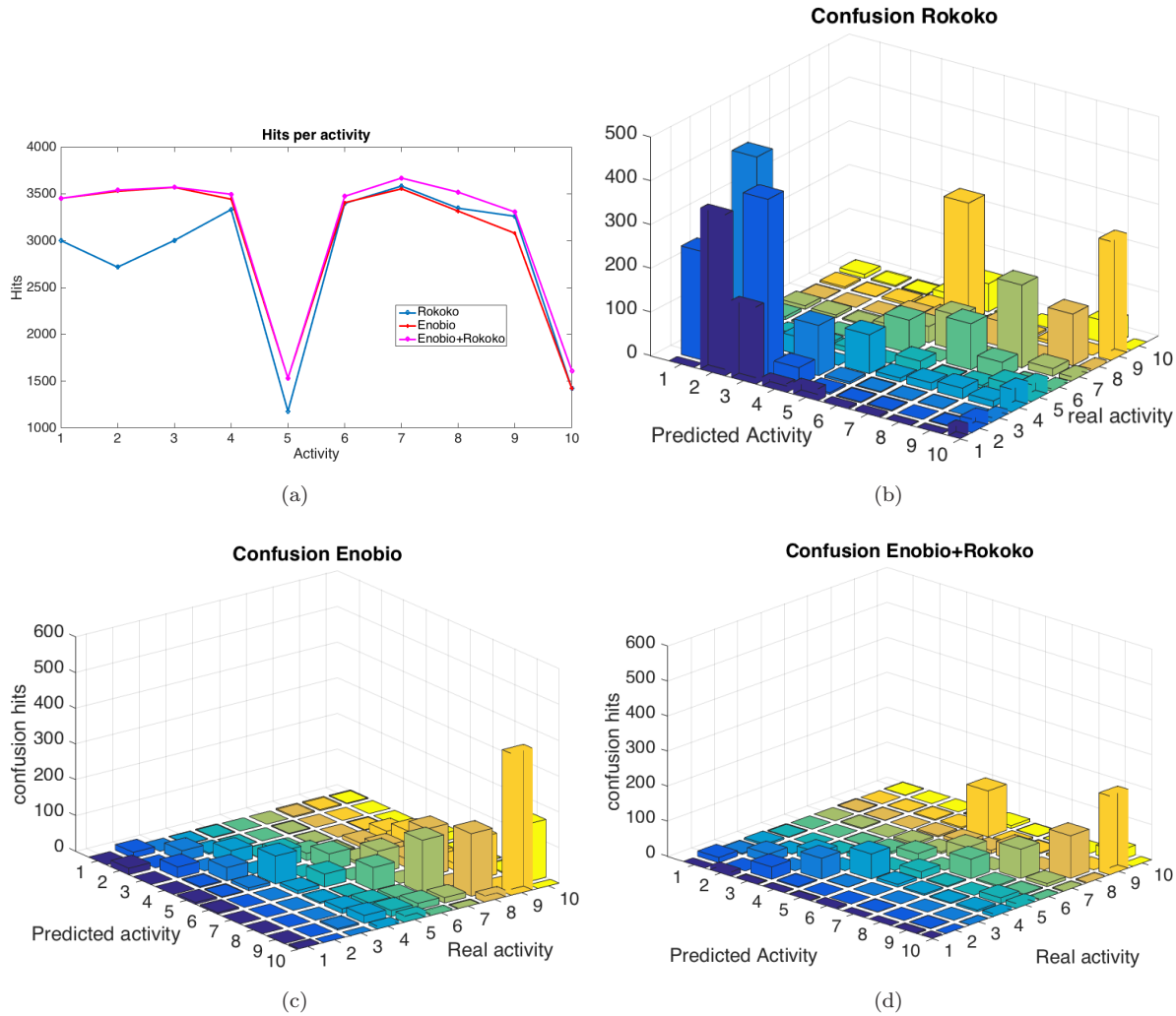

Fig. 8. Summary of the ethogram computation on the out-house experiment data. (a) Correct predictions per activity, (b) confusion matrix on the inertial (rokoko) data, (c) confusion matrix on the EEG (enobio) data, and (d) confusion matrix on the sensor fusion data.

the accuracy of ethogram inference on the same set, they are significantly higher and less variable than in the in-house case (mean = 0.968, std. dev. = 0.018, two sample t-test $p < 0.001$). This improvement may be due to the enhanced experimental deployment as the research team experience increases. The off diagonal values correspond to the transfer learning accuracy, they are significantly lower (mean = 0.76, std. dev. = 0.03) than the accuracy values on the diagonal (two sample t-test, $p < 1e-10$). We note that the degradation of the transfer learning accuracy is smaller when the transfer is to the other repetition of the same subject (mean = 0.88, std. dev. = 0.01). This difference is statistically significant (one side t-test, $p < 1e-5$).

4. Discussion

Our work touches quite different emerging fields, on the one hand, the human activity recognition field, and on the other hand, the mobile brain imaging (MBI) field. Human activity recognition has been developed mostly using computer vision techniques over optical sensors data,[1,68] however there is a growing body of research based on wearable sensors.[69,70] Data fusion for human activity recognition often refers to same kind of sensors, e.g. the fusion of IMUs tracking data in Ref. 70. To our knowledge, there has not been any previous attempt to apply the fusion of EEG and other sensor data. In this paper, we have achieved the recognition of a sequence of activities

Table 2. Transfer learning results for the out-house protocol repetitions. Each row corresponds to the accuracy achieved applying the best classifier trained on the data of a protocol repetition to the remaining repetitions. Repetitions are denoted Tx-y, x = subject id, y = repetition number. Post-processing time correction was applied.

	T0-0	T0-1	T2-0	T2-1	T3-0	T3-1	T4-0	T4-1	T5-0	T6-0	T6-1	T7-0	T7-1	T9-1	T10-0	T10-1	T11-0	T11-1
T0-0	0.98	0.90	0.77	0.79	0.78	0.79	0.77	0.76	0.75	0.76	0.74	0.77	0.75	0.77	0.76	0.75	0.77	0.76
T0-1	0.90	0.97	0.76	0.78	0.79	0.77	0.75	0.77	0.75	0.74	0.73	0.77	0.76	0.78	0.77	0.73	0.78	0.79
T2-0	0.78	0.77	0.97	0.89	0.75	0.77	0.73	0.73	0.76	0.75	0.8	0.77	0.78	0.77	0.75	0.74	0.72	0.72
T2-1	0.80	0.79	0.89	0.98	0.80	0.79	0.75	0.74	0.77	0.79	0.79	0.76	0.77	0.75	0.74	0.72	0.72	0.72
T3-0	0.77	0.78	0.77	0.79	0.98	0.90	0.77	0.73	0.77	0.78	0.77	0.75	0.79	0.74	0.74	0.73	0.73	0.74
T3-1	0.78	0.76	0.78	0.79	0.89	0.98	0.71	0.76	0.75	0.74	0.73	0.75	0.77	0.75	0.73	0.78	0.77	0.77
T4-0	0.79	0.77	0.72	0.75	0.72	0.76	0.97	0.88	0.84	0.75	0.78	0.74	0.76	0.76	0.78	0.78	0.73	0.73
T4-1	0.75	0.74	0.72	0.75	0.76	0.78	0.89	0.97	0.84	0.74	0.75	0.76	0.74	0.77	0.77	0.77	0.74	0.74
T5-0	0.77	0.75	0.76	0.76	0.75	0.74	0.85	0.85	0.98	0.75	0.73	0.75	0.71	0.75	0.76	0.74	0.73	0.72
T6-0	0.76	0.75	0.76	0.78	0.73	0.75	0.75	0.73	0.75	0.99	0.89	0.77	0.77	0.75	0.77	0.78	0.77	0.76
T6-1	0.77	0.76	0.79	0.77	0.72	0.78	0.73	0.74	0.75	0.90	0.98	0.77	0.78	0.76	0.78	0.78	0.78	0.79
T7-0	0.75	0.76	0.75	0.77	0.75	0.75	0.75	0.77	0.77	0.78	0.77	0.96	0.88	0.76	0.74	0.74	0.75	0.75
T7-1	0.74	0.74	0.77	0.78	0.73	0.77	0.74	0.76	0.77	0.77	0.77	0.86	0.91	0.76	0.75	0.75	0.75	0.75
T9-1	0.77	0.77	0.79	0.79	0.75	0.76	0.75	0.76	0.75	0.76	0.77	0.76	0.75	0.95	0.73	0.72	0.72	0.73
T10-0	0.77	0.78	0.76	0.72	0.78	0.79	0.77	0.77	0.77	0.78	0.78	0.75	0.74	0.72	0.96	0.87	0.73	0.72
T10-1	0.76	0.76	0.77	0.72	0.73	0.76	0.77	0.75	0.76	0.78	0.78	0.75	0.74	0.72	0.86	0.96	0.73	0.73
T11-0	0.77	0.76	0.73	0.74	0.74	0.71	0.75	0.75	0.75	0.79	0.79	0.74	0.75	0.72	0.73	0.73	0.99	0.89
T11-1	0.75	0.75	0.74	0.75	0.75	0.71	0.75	0.75	0.74	0.79	0.79	0.75	0.74	0.72	0.73	0.73	0.90	0.96

mixing cognitive and motor tasks, where the EEG data play a complementary role to the IMUs data.

The dominant paradigm in EEG-based cognitive research is defined by the event-related potential (ERP) techniques,[71] where short EEG signal intervals following a controlled event are filtered and averaged looking for specific signal patterns corresponding to stereotypic electrophysiological response of the brain to an stimulus. Analysis of the ERP structure (peaks and valleys) allows to infer the underlying brain function. The work reported in this paper does not fit in this paradigm as long as we do not have specific stimuli applied to the subject and we do not extract and average small chunks of the EEG signal. Instead, we filter the entire signals, and use their instantaneous values as features for activity recognition in a sequential protocol.

The advent of wireless EEG devices has set the stage for the mobile brain imaging (MBI) field, which has a very broad definition as a meeting point of neuroscience, arts, and human computer interaction.[72] In more concrete terms, MBI research is aiming to greater ecological validity allowing for less constrained experimental environments, where the subjects can be doing some natural movements like walking or pedaling. Recent MBI research has focused on the reproducibility of ERPs while the subject is moving, comparing static and moving signal analysis results. Some works study the auditive odd-ball task ERPs while sitting versus pedaling.[73,74] In an other study,[75] subjects carry out an inhibitory task while walking versus sitting. Other studies include the analysis of pianists EEG ERPs and power spectrum while performing a simple tune,[57] the prediction of braking intention from ERPs,[76] and the effect of rhythmic auditory stimulation on auditory motor synchronization on Parkinson's disease patients.[77] New datasets are being published in order to stimulate computational research in this exciting new area.[78] However, these studies do not try to analyze neural activity and behavior measurements together, as a wholistic measurement. Our fused inertial plus EEG signal classification results show that using the joint information improves over the separate sources of information, achieving activity recognition accuracies over 0.9, which are much higher than the accuracies achieved in ERP classification for brain computer interaction.[72] Besides, our focus is the wholistic recognition of the neuroethogram (the ethogram inferred from neural and behavioral measurements) instead of the reaction to specific atomic events following neuroethological approaches already studied on animal models.[49] In this regard, future work will be devoted to the

recognition of neuroethogram patterns, and characterization of deviations related with neural disorders or diseases. We are interested in the development of tools for the study of how some treatments affect subjects with some form or another of neural diseases,[79] elderly,[80] or children with special needs.[81] Many of these conditions show typical external behavioral traits that can be objectively measured by means of motion capture devices, allowing to measure changes in behavior due to treatment with great accuracy. For instance, children with autism spectrum condition (ASC) often show stereotypical behaviors[82] whose neural correlates are far from understood. We think that the analysis of the neuroethograms will be a fruitful avenue of research on these issues.

Limitations. The data sample size is small so the study does not allow general conclusions. However, our sample is greater than those of recently published works on mobile EEG.[73,74,76] The gender representation is quite imbalanced, hence it is not possible to carry out any gender-related contrast analysis. We have carried out the data capture sessions inside rooms without working electrical equipment, but we have not ensured total electromagnetic isolation, i.e. by carrying out the experiment inside a Faraday cage. Cognitive EEG experiments are composed of a large number of repetitions of very short experiments, i.e. with durations in the order of seconds, whose neural patterns are averaged to remove noise and obtain the evoked potentials for further analysis. Our data capture sessions did not follow this pattern, we have long unique trial recordings with rough synchronization among them, which cannot be treated as ERPs. Finally, results might improve when larger populations are recruited for data capture.

5. Conclusions and Future Work

In this paper, we have introduced a system composed of IMUs and EEG recording, both wirelessly connected, which allows subjects to carry out natural activities while being recorded. We demonstrate on an experimental data capture protocol that the fusion of inertial motion and neural activity information provides improved activity classification capabilities, opening another door for neuroethological research works at the human level. Future works will be aiming to adapt the system to experimental settings that can be used for actual evaluation of treatments on patients with neurological affections through the wholistic analysis of the neuroethograms computed from the fusion of EEG and IMU data.

Acknowledgments

This work has been partially supported by FEDER funds through MINECO Project TIN2017-85827-P. Special thanks to Naiara Vidal from IMH who conducted the recruitment process in the framework of Langileok project funded by the Elkartek program. This project has received funding from the European Union's Horizon 2020 research and innovation programme under the Marie Sklodowska-Curie grant agreement No. 777720.

References

1. M. Vrigkas, C. Nikou and I. A. Kakadiaris, A review of human activity recognition methods, *Front. Robot. AI* **2** (2015) 28.
2. J. Shotton, A. Fitzgibbon, M. Cook, T. Sharp, M. Finocchio, R. Moore, A. Kipman and A. Blake, Real-time human pose recognition in parts from single depth images, in *Machine Learning for Computer Vision*, eds. R. Cipolla, S. Battiato and G. M. Farinella (Springer, Berlin, Heidelberg, 2013), pp. 119–135.
3. E. E. Stone and M. Skubic, Unobtrusive, continuous, in-home gait measurement using the microsoft kinect, *IEEE Trans. Biomed. Eng.* **60** (2013) 2925–2932.
4. A. Mannini and A. M. Sabatini, Machine learning methods for classifying human physical activity from on-body accelerometers, *Sensors* **10**(2) (2010) 1154–1175.
5. S. Obdrzalek, G. Kurillo, F. Ofli, R. Bajcsy, E. Seto, H. Jimison and M. Pavel, Accuracy and robustness of kinect pose estimation in the context of coaching of elderly population, in *Annual Int. Conf. IEEE Engineering in Medicine and Biology Society* (IEEE, 2012), pp. 1188–1193.
6. J.-Y. Yang, J.-S. Wang and Y.-P. Chen, Using acceleration measurements for activity recognition: An effective learning algorithm for constructing neural classifiers, *Pattern Recogn. Lett.* **29**(16) (2008) 2213–2220.
7. H. Zeng and Y. Zhao, Sensing movement: Microsensors for body motion measurement, *Sensors* **11**(1) (2011) 638–660.
8. M. Airaksinen, O. Räsänen, E. Ilén, T. Häyrinen, A. Kivi, V. Marchi, A. Gallen, S. Blom, A. Varhe, N. Kaartinen, L. Haataja and S. Vanhatalo, Automatic posture and movement tracking of infants with wearable movement sensors, *Sci. Rep.* **10**(1) (2020) 169.

9. J. Wang, R. Chen, X. Sun, M. F. She and Y. Wu, Recognizing human daily activities from accelerometer signal, *Procedia Eng.* **15** (2011) 1780–1786.
10. K. H. Beange, A. D. Chan, S. M. Beaudette and R. B. Graham, Concurrent validity of a wearable imu for objective assessments of functional movement quality and control of the lumbar spine, *J. Biomech.* **97** (2019) 109356.
11. W. D. Kearns, J. L. Fozard and V. O. Nams, Movement path tortuosity in free ambulation: Relationships to age and brain disease, *IEEE J. Biomed. Health Inf.* **21** (2017) 539–548.
12. M. Blank, L. Gorelick, E. Shechtman, M. Irani and R. Basri, Actions as space-time shapes, *Tenth IEEE Int. Conf. Computer Vision* (*ICCV'05*) *Volume 1*, Vol. 2 (Beijing, China, IEEE Press, 2005), pp. 1395–1402.
13. C. Sminchisescu, A. Kanaujia, Z. Li and D. Metaxas, Conditional models for contextual human motion recognition, *Tenth IEEE Int. Conf. Computer Vision (ICCV'05) Volume 1*, Vol. 2 (Beijing, China, IEEE Press, 2005), pp. 1808–1815.
14. A. A. Aguileta, R. F. Brena, O. Mayora, E. Molino-Minero-Re and L. A. Trejo, Multi-sensor fusion for activity recognition — a survey, *Sensors* **19**(17) (2019) 3808.
15. H. F. Nweke, Y. W. Teh, G. Mujtaba and M. A. Algaradi, Data fusion and multiple classifier systems for human activity detection and health monitoring: Review and open research directions, *Inf. Fusion* **46** (2019) 147–170.
16. S. Chung, J. Lim, K. J. Noh, G. Kim and H. Jeong, Sensor data acquisition and multimodal sensor fusion for human activity recognition using deep learning, *Sensors* **19**(7) (2019) 1716.
17. D. J. Anderson and P. Perona, Toward a science of computational ethology, *Neuron* **84**(1) (2014) 18–31.
18. B. E. Jackson, D. J. Evangelista, D. D. Ray and T. L. Hedrick, 3d for the people: Multi-camera motion capture in the field with consumer-grade cameras and open source software, *Biol. Open* **5**(9) (2016) 1334–1342.
19. A. I. Dell, J. A. Bender, K. Branson, I. D. Couzin, G. G. de Polavieja, L. P. J. J. Noldus, A. Pérez-Escudero, P. Perona, A. D. Straw, M. Wikelski and U. Brose, Automated image-based tracking and its application in ecology, *Trends Ecol. Evol.* **29** (2014) 417–428.
20. M. Saberioon and P. Cisar, Automated multiple fish tracking in three-dimension using a structured light sensor, *Comput. Electron. Agric.* **121** (2016) 215–221.
21. H. Jhuang, E. Garrote, X. Yu, V. Khilnani, T. Poggio, A. D. Steele and T. Serre, Automated home-cage behavioural phenotyping of mice, *Nat. Commun.* **1** (2010) 68.
22. A. Iyengar, J. Imoehl, A. Ueda, J. Nirschl and C.-F. Wu, Automated quantification of locomotion, social interaction, and mate preference in drosophila mutants, *J. Neurogenet.* **26** (2012) 306–316.
23. A. Weissbrod, A. Shapiro, G. Vasserman, L. Edry, M. Dayan, A. Yitzhaky, L. Hertzberg, O. Feinerman and T. Kimchi, Automated long-term tracking and social behavioural phenotyping of animal colonies within a semi-natural environment, *Nat. Commun.* **4** (2013) 2018.
24. M. Kabra, A. A. Robie, M. Rivera-Alba, S. Branson and K. Branson, Jaaba: Interactive machine learning for automatic annotation of animal behavior, *Nat. Methods* **10** (2012) 64.
25. A. Spink, R. Tegelenbosch, M. Buma and L. Noldus, The ethovision video tracking system — A tool for behavioral phenotyping of transgenic mice, *Physiol. Behav.* **73**(5) (2001) 731–744.
26. X. P. Burgos-Artizzu, P. Dollár, D. Lin, D. J. Anderson and P. Perona, Social behavior recognition in continuous video, *2012 IEEE Conf. Computer Vision and Pattern Recognition* (Providence, Rhode Island, 2012), pp. 1322–1329.
27. M. I. Carreno, K. L. de Ipiña, B. Beitia, A. Moujahid, M. I. Carreno, A. Frick and X. Leinekugel, First approach to the analysis of spontaneous activity of mice based on permutation entropy, *2015 4th Int. Work Conf. Bioinspired Intelligence (IWOBI)* (San Sebastian, Spain, 2015), pp. 197–204.
28. H. Fröhlich, K. Claes, C. D. Wolf, X. V. Damme and A. Michel, A machine learning approach to automated gait analysis for the noldus catwalk system, *IEEE Trans. Biomed. Eng.* **65** (2018) 1133–1139.
29. B. Akkaya, Y. Tabar, F. Gharbalchi, I. Ulusoy and U. Halici, Tracking mice face in video, *20th National Biomedical Engineering Meeting* (*BIYOMUT*) (Izmir, Turkey, 2016), pp. 1–4.
30. A. Ortiz, J. Munilla, J. M. Gorriz and J. Ramirez, Ensembles of deep learning architectures for the early diagnosis of the alzheimer's disease, *Int. J. Neural Syst.* **26**(7) (2016) 1650025.
31. İ. B. Akkaya and U. Halici, Mouse face tracking using convolutional neural networks, *IET Comput. Vis.* **12**(2) (2018) 153–161.
32. Z. Reznikova, J. Levenets, S. Panteleeva and B. Ryabko, Studying hunting behaviour in the striped field mouse using data compression, *Acta Ethol.* **20** (2017) 165–173.
33. W. O. Tatum, *Handbook of EEG Interpretation* (Demos Medical Publishing, 2014).
34. T. Alotaiby, F. E. A. El-Samie, S. A. Alshebeili and I. Ahmad, A review of channel selection algorithms for eeg signal processing, *EURASIP J. Adv. Signal Process.* **2015** (2015) 66.
35. O. Bazanova and D. Vernon, Interpreting eeg alpha activity, *Neurosci. Biobehav. Rev.* **44** (2014) 94–110.

36. W. Klimesch, Eeg alpha and theta oscillations reflect cognitive and memory performance: A review and analysis, *Brain Res. Rev.* **29**(2) (1999) 169–195.
37. V. V. Vyazovskiy and I. Tobler, Theta activity in the waking eeg is a marker of sleep propensity in the rat, *Brain Res.* **1050**(1) (2005) 64–71.
38. A. Fernández-Soto, A. Martínez-Rodrigo, J. Moncho-Bogani, J. M. Latorre and A. Fernández-Caballero, Neural correlates of phrase quadrature perception in harmonic rhythm: An eeg study using a brain–computer interface, *Int. J. Neural Syst.* **28**(5) (2018) 1750054.
39. M. Brewer, Research design and issues of validity, *Handbook of Research Methods in Social and Personality Psychology*, eds. H. Reis and C. E. Judd (Cambridge University Press, Cambridge, 2000).
40. A. C. Grant, S. G. Abdel-Baki, A. Omurtag, R. Sinert, G. Chari, S. Malhotra, J. Weedon, A. A. Fenton and S. Zehtabchi, Diagnostic accuracy of microeeg: A miniature, wireless eeg device, *Epilepsy Behav.* **34** (2014) 81–85.
41. J. W. Kam, S. Griffin, A. Shen, S. Patel, H. Hinrichs, H.-J. Heinze, L. Y. Deouell and R. T. Knight, Systematic comparison between a wireless eeg system with dry electrodes and a wired eeg system with wet electrodes, *NeuroImage* **184** (2019) 119–129.
42. J. M. Rogers, S. J. Johnstone, A. Aminov, J. Donnelly and P. H. Wilson, Test-retest reliability of a single-channel, wireless eeg system, *Int. J. Psychophysiol.* **106** (2016) 87–96.
43. K. A. Davis, B. K. Sturges, C. H. Vite, V. Ruedebusch, G. Worrell, A. B. Gardner, K. Leyde, W. D. Sheffield and B. Litt, A novel implanted device to wirelessly record and analyze continuous intracranial canine eeg, *Epilepsy Res.* **96**(1) (2011) 116–122.
44. N. Perentos, A. Nicol, A. Martins, J. Stewart, P. Taylor and A. Morton, Techniques for chronic monitoring of brain activity in freely moving sheep using wireless eeg recording, *J. Neurosci. Methods* **279** (2017) 87–100.
45. E. Ratti, S. Waninger, C. Berka, G. Ruffini and A. Verma, Comparison of medical and consumer wireless eeg systems for use in clinical trials, *Front. Hum. Neurosci.* **11** (2017) 398.
46. J. G. Cruz-Garza, J. A. Brantley, S. Nakagome, K. Kontson, M. Megjhani, D. Robleto and J. L. Contreras-Vidal, Deployment of mobile eeg technology in an art museum setting: Evaluation of signal quality and usability, *Front. Hum. Neurosci.* **11** (2017) 527.
47. N. S. Dias, J. P. Carmo, P. M. Mendes and J. H. Correia, Wireless instrumentation system based on dry electrodes for acquiring eeg signals, *Med. Eng. Phys.* **34**(7) (2012) 972–981.
48. G. Hoyle, The scope of neuroethology, *Behav. Brain Sci.* **7** (1984) 367–412 .
49. J. T. Vogelstein, Y. Park, T. Ohyama, R. A. Kerr, J. W. Truman, C. E. Priebe and M. Zlatic, Discovery of brainwide neural-behavioral maps via multiscale unsupervised structure learning, *Science* **344**(6182) (2014) 386–392.
50. M. Fournely, Y. Petit, É. Wagnac, J. Laurin, V. Callot and P.-J. Arnoux, High-speed video analysis improves the accuracy of spinal cord compression measurement in a mouse contusion model, *J. Neurosci. Methods* **293** (2018) 1–5.
51. B. Tang, D. Wang, M. Li, Q. Wu, Q. Yang, W. Shi and C. Chen, An in vivo study of hypoxia-inducible factor-1α signaling in ginsenoside rg1-mediated brain repair after hypoxia/ischemia brain injury, *Pediatr. Res.* **81** (2016) 120.
52. D. Mobbs and J. J. Kim, Neuroethological studies of fear, anxiety, and risky decision-making in rodents and humans, *Cur. Opin. Behav. Sci* **5** (2015) 8–15.
53. D. Mobbs, D. Hassabis, R. Yu, C. Chu, M. Rushworth, E. Boorman and T. Dalgleish, Foraging under competition: The neural basis of input-matching in humans, *J. Neurosci.* **33**(23) (2013) 9866–9872.
54. O. M. Mozos, V. Sandulescu, S. Andrews, D. Ellis, N. Bellotto, R. Dobrescu and J. M. Ferrandez, Stress detection using wearable physiological and sociometric sensors, *Int. J. Neural Syst.* **27**(2) (2017) 1650041.
55. M.-C. Corsi, M. Chavez, D. Schwartz, L. Hugueville, A. N. Khambhati, D. S. Bassett and F. De Vico Fallani, Integrating eeg and meg signals to improve motor imagery classification in brain–computer interface, *Int. J. Neural Syst.* **29**(1) (2019) 1850014.
56. Q. Yuan, W. Zhou, F. Xu, Y. Leng and D. Wei, Epileptic eeg identification via lbp operators on wavelet coefficients, *Int. J. Neural Syst.* **28**(8) (2018) 1850010.
57. A. Zamm, C. Palmer, A.-K. R. Bauer, M. G. Bleichner, A. P. Demos and S. Debener, Synchronizing midi and wireless eeg measurements during natural piano performance, *Brain Res.* **1716** (2019) 27–38.
58. I. B. Araquistain, X. Garmendia, M. Graña and J. de Lope Asiain, Fusion of inertial motion sensors and electroencephalogram for activity detection, in *Understanding the Brain Function and Emotions*, eds. J. M. Ferrandez, J. M. Vicente, J. R. Alvarez-Sanchez, F. de la Paz Lopez, J. Toledo Moreo and H. Adeli (Springer International Publishing, Cham, 2019), pp. 319–326.
59. I. Baglietto, X. Garmendia and M. Graña, A synchronized capture system for Emotiv+, Kinect, and Rokoko motion capture, https://doi.org/10.5281/zenodo.2548964 (2019).
60. R. T. T. Hastie and J. Friedman, *Elements of Statistical Learning* (Springer, 2009).
61. L. Breiman, J. Friedman, R. Olshen and C. Stone, *Classification and Regression Trees* (Wadsworth, Belmont, CA, 1984).

62. L. Breiman, Random forests, *Mach. Learn.* **45**(1) (2001) 5–32.
63. J. Friedman, Greedy function approximation: A gradient boosting machine, *Ann. Stat.* **29**(5) (2001) 1189–1232.
64. M. Fernández-Delgado, E. Cernadas, S. Barro and D. Amorim, Do we need hundreds of classifiers to solve real world classification problems?, *J. Mach. Learn. Res.* **15**(90) (2014) 3133–3181.
65. M. Wainberg, B. Alipanahi and B. J. Frey, Are random forests truly the best classifiers?, *J. Mach. Learn. Res.* **17**(110) (2016) 1–5.
66. A. Natekin and A. Knoll, Gradient boosting machines, a tutorial, *Front. Neurorobot.* **7** (2013) 21.
67. D. J. Hand and K. Yu, Idiot's bayes: Not so stupid after all?, *Int. Stat. Rev.* **69**(3) (2001) 385–398.
68. H. Mliki, F. Bouhlel and M. Hammami, Human activity recognition from uav-captured video sequences, *Pattern Recognit.* **100** (2020) 107140.
69. J. Wang, Y. Chen, S. Hao, X. Peng and L. Hu, Deep learning for sensor-based activity recognition: A survey, *Pattern Recognit. Lett.* **119** (2019) 3–11.
70. Z. Qin, Y. Zhang, S. Meng, Z. Qin and K.-K. R. Choo, Imaging and fusing time series for wearable sensor-based human activity recognition, *Inf. Fusion* **53** (2020) 80–87.
71. S. Luck, *An Introduction to the Event-Related Potential Technique* (The MIT Press, Boston, MA, 2005).
72. J. L. Contreras-Vidal, D. Robleto, J. G. Cruz-Garza, J. M. Azorín and C. Nam, *Mobile Brain-Body Imaging and the Neuroscience of Art, Innovation and Creativity* (Springer International Publishing, Cham, SW, 2019).
73. S. Blum, S. Debener, R. Emkes, N. Volkening, S. Fudickar and M. Bleichner, Eeg recording and online signal processing on android: A multiapp framework for brain-computer interfaces on smartphone, *BioMed Res. Int.* **2017** (2017) 3072870.
74. J. E. Scanlon, K. A. Townsend, D. L. Cormier, J. W. Kuziek and K. E. Mathewson, Taking off the training wheels: Measuring auditory p3 during outdoor cycling using an active wet eeg system, *Brain Res.* **1716** (2019) 50–61.
75. B. R. Malcolm, J. J. Foxe, J. S. Butler, W. B. Mowrey, S. Molholm and P. D. Sanctis, Long-term test-retest reliability of event-related potential (erp) recordings during treadmill walking using the mobile brain/body imaging (mobi) approach, *Brain Res.* **1716** (2019) 62–69.
76. G. Vecchiato, M. D. Vecchio, L. Ascari, S. Antopolskiy, F. Deon, L. Kubin, J. Ambeck-Madsen, G. Rizzolatti and P. Avanzini, Electroencephalographic time-frequency patterns of braking and acceleration movement preparation in car driving simulation, *Brain Res.* **1716** (2019) 16–26.
77. J. Lei, N. Conradi, C. Abel, S. Frisch, A. Brodski-Guerniero, M. Hildner, C. A. Kell, J. Kaiser and M. Schmidt-Kassow, Cognitive effects of rhythmic auditory stimulation in parkinson's disease: A p300 study, *Brain Res.* **1716** (2019) 70–79.
78. J. Wagner, R. Martinez-Cancino, A. Delorme, S. Makeig, T. Solis-Escalante, C. Neuper and G. Mueller-Putz, High-density eeg mobile brain/body imaging data recorded during a challenging auditory gait pacing task, *Sci. Data* **6**(1) (2019) 211.
79. M. Graña, L. Ozaeta and D. Chyzhyk, Resting state effective connectivity allows auditory hallucination discrimination, *Int. J. Neural Syst.* **27**(5) (2017) 1750019.
80. J. M. Lopez-Guede, A. Moreno-Fernandez-de Leceta, A. Martinez-Garcia and M. Graña, Lynx: Automatic elderly behavior prediction in home telecare, *BioMed Res. Int.* **2015** (2015) 18.
81. M. Graña, On the proposed cybspeed project experimental research protocols, Zenodo, https://doi.org.10.5281/zenodo.1405505 (2018).
82. A. d'Anjou, M. Graña and F. Moutet, Brief survey about the search for biomarkers and computer aided diagnosis of autism spectrum disorder, zenodo (2018), http://doi.org/10.5281/zenodo.1408202.